

A Novel Scenario in the Semi-constrained NMSSM

Kun Wang and Jingya Zhu

*Center for Theoretical Physics, School of Physics and Technology, Wuhan University,
Wuhan 430072, China*

E-mail: wk2016@whu.edu.cn, zhuji@whu.edu.cn

ABSTRACT: In this work, we develop a novel efficient scan method, combining the Heuristically Search (HS) and the Generative Adversarial Network (GAN), where the HS can shift marginal samples to perfect samples, and the GAN can generate a huge amount of recommended samples from noise in a short time. With this efficient method, we find a new scenario in the semi-constrained Next-to Minimal Supersymmetric Standard Model (scNMSSM), or NMSSM with non-universal Higgs masses. In this scenario, (i) Both muon $g-2$ and right relic density can be satisfied, along with the high mass bound of gluino, etc. As far as we know, that had not been realized in the scNMSSM before this work. (ii) With the right relic density, the lightest neutralinos are singlino-dominated, and can be as light as 0-12 GeV. (iii) The future direct detections XENONnT and LUX-ZEPLIN (LZ-7 2T) can give strong constraints to this scenario. (iv) The current indirect constraints to Higgs invisible decay $h_2 \rightarrow \tilde{\chi}_1^0 \tilde{\chi}_1^0$ are weak, but the direct detection of Higgs invisible decay at the future HL-LHC may cover half of the samples, and that of the CEPC may cover most. (v) The branching ratio of Higgs exotic decay $h_2 \rightarrow h_1 h_1, a_1 a_1$ can be over 20 percent, while their contributions ($h_2 \rightarrow 4\tilde{\chi}_1^0$) to the invisible decay are very small.

Contents

1	Introduction	1
2	The semi-constrained NMSSM and the search strategy	2
2.1	The Higgs and electroweakinos sector of the scNMSSM	3
2.2	The Heuristically Search (HS)	5
2.3	The Generative Adversarial Network (GAN)	7
3	Results and discussions	7
3.1	Scan with HS and GAN	8
3.2	Light dark matter (DM) and Higgs invisible decay	12
4	Conclusions	18

1 Introduction

Higgs boson was discovered in 2012 [1, 2], and its production rate in most channels coincides with the Standard Model (SM) prediction considering uncertainties [3–5]. While there are still chances for physics beyond the SM. For example, for the branching ratio of Higgs boson invisible decay, the current excluding limits are only 26% by ATLAS [6] and 19% by CMS [7], with all data at Run I and data of about 36 fb^{-1} at Run II.

Supersymmetry is a popular theory beyond the SM, which introduces a new internal symmetry between fermions and bosons. Thus the large hierarchy problem can be solved, gauge coupling can be unified, and dark matter (DM) candidates can be provided, etc. In the Minimal supersymmetric Standard Model (MSSM) with 7 free parameters at the electroweak scale, a SM-like 125 GeV Higgs can be afforded, but need large fine-tuning, and the branching ratio of Higgs boson invisible decay can be about 10% at most [8–10]. The Next-to Minimal Supersymmetric Standard Model (NMSSM) with \mathbb{Z}_3 symmetry extends the MSSM by a complex singlet superfield \hat{S} , but introduces four more parameters. In the graceful and simple model of fully-constrained NMSSM (cNMSSM), all Higgs and sfermion masses are assumed to be unified at the Grand Unified theoretical (GUT) scale, thus only four parameters at GUT scale are left free [11–19]. These four or five parameters run according to the Renormalization Group Equations (RGEs), forming the spectrum of NMSSM at low energy scale. While it was found that when considering all the constraints including muon g-2, the SM-like Higgs mass can not reach to 125 GeV in the cNMSSM¹ [11, 12], like these in the CMSSM, NUHM1 and NUHM2 [21–24].

¹Notice that there are also some other ways to solve this problem, e.g., introducing right-handed neutrinos to the cNMSSM [20].

In this work, we consider possible scenarios of Higgs invisible decay in the semi-constrained NMSSM (scNMSSM) [25–30], which relaxing the Higgs masses at the GUT scale, and also called NMSSM with non-universal Higgs mass (NUHM). As a simple and graceful SUSY model, the scNMSSM had attracted much attention. In Refs.[27, 28] the constraints of LHC and dark matter to scNMSSM was considered, while the muon g-2 was left aside; in Ref.[26] muon g-2 was satisfied, while dark matter relic density is not sufficient; In Refs.[25, 29, 30], direct searches for the higgsino sector was considered; In Ref.[31], the extended model with right-handed neutrinos was considered. In this work, we consider all constraints including muon g-2, and also try to get sufficient relic density.

In this work, to include constraints of muon g-2, etc., get sufficient relic density, and get as-large-as-possible branching ratio of Higgs invisible decay, we developed a novel efficient method to scan the parameter space, which consists of the Heuristically Search (HS) and the Generative Adversarial Network (GAN). Note that in Refs.[32, 33], the Machine Learning (ML) scan method has been used to explore the parameter space, and a scanning tool xBIT [34] based on ML has been developed. This ML scan is based on several classifiers, dealing with a Classification problem that each sample gets a probability of how much it could be a perfect sample. This scan method also needs to generate samples in high-dimension space, which will cost very long time, (eg., when the dimension is 9 and each dimension has 100 grid, at least 100^9 samples need to be generated). On the contrary, we adopt a generative model, the Generative Adversarial Network (GAN) [35], which is a famous star in deep learning area and also gets much attention in high energy physics [36–44]. The GAN can directly generate samples with the similar distribution as the training samples. So with a well-trained GAN, we can get as many recommended samples as we want. And with the HS we developed, we have a chance to shift some ‘bad’ or ‘marginal’ samples to ‘good’ samples. Combined with HS and GAN, we developed a novel method that can get a huge mount of surviving samples in a short time. Then, we used this novel efficient method to study the parameter space of scNMSSM, under current constraints including LHC, B physics, muon g-2, and dark matter, etc. We require our surviving samples to satisfy all these constraints, and part of them predict right relic density. To study Higgs invisible decay, we require the LSP mass lighter than half of the SM-like Higgs mass ($m_{\tilde{\chi}_1^0} < m_{h_{\text{SM}}}/2$), and the invisible branching ratio be as large as possible. As can be seen from the following sections, this method is powerful in getting this novel scenario in the scNMSSM.

The rest of this paper is organized as follows. In section 2, we briefly introduce the Higgs and electroweakino sectors of the scNMSSM, and our search strategy consisting of HS and GAN. In section 3, we describe the detail of our scan process and then discuss the Higgs invisible decay and light dark matter in the scNMSSM. Finally, we draw our conclusions in section 4.

2 The semi-constrained NMSSM and the search strategy

The NMSSM extends the MSSM particle content by adding a singlet superfield \hat{S} , which provides an effective μ -term. The superpotential of the \mathbb{Z}_3 -invariant NMSSM is

$$W_{\text{NMSSM}} = y_u \hat{Q} \cdot \hat{H}_u \hat{u}^c + y_d \hat{Q} \cdot \hat{H}_d \hat{d}^c + y_u \hat{L} \cdot \hat{H}_d \hat{e}^c + \lambda \hat{S} \hat{H}_u \cdot \hat{H}_d + \frac{\kappa}{3} \hat{S}^3 \quad (2.1)$$

where the hats are used for superfields, $y_{u,d,e}$ stand for corresponding Yukawa couplings, and λ, κ are dimensionless coupling constants. When the singlet superfield \hat{S} gets a vacuum expectation value (VEV), $\langle S \rangle = v_s$, a effective μ -term is generated dynamically from the term $\lambda \hat{S} \hat{H}_u \cdot \hat{H}_d$, with

$$\mu_{\text{eff}} = \lambda v_s. \quad (2.2)$$

For convenience, in the following we refer to μ_{eff} as μ . And the VEVs of the two doublet Higgs superfields \hat{H}_u and \hat{H}_d are v_u and v_d respectively, where $v_u^2 + v_d^2 = v^2 = (174 \text{ GeV})^2$.

The soft SUSY breaking terms in the NMSSM are only different from the MSSM in several terms:

$$-\mathcal{L}_{\text{NMSSM}}^{\text{soft}} = -\mathcal{L}_{\text{MSSM}}^{\text{soft}}|_{\mu=0} + m_S^2 |S|^2 + \lambda A_\lambda S H_u \cdot H_d + \frac{1}{3} \kappa A_\kappa S^3 + h.c., \quad (2.3)$$

where the S , H_u and H_d are the scalar components of the superfields respectively, the m_S^2 is the soft SUSY breaking mass for single field S , and the trilinear coupling constants A_λ and A_κ have mass dimension.

Unlike that in the CNMSSM or CMSSM, in the scNMSSM the Higgs sector is assumed to be non-universal at the GUT scale. Then, at the GUT scale, the Higgs soft mass $m_{H_u}^2, m_{H_d}^2$ and m_S^2 are allowed to be different from $M_0^2 + \mu^2$, and the trilinear couplings A_λ, A_κ can be different from A_0 . Hence, in the scNMSSM, the complete parameter sector can be usually chosen as

$$\lambda, \kappa, \tan\beta = \frac{v_u}{v_d}, \mu, A_\lambda, A_\kappa, A_0, M_{1/2}, M_0 \quad (2.4)$$

at the GUT scale. While the parameters at low energy scale can be calculated in the RGEs running from these GUT-scale parameters.

2.1 The Higgs and electroweakinos sector of the scNMSSM

When the electroweak symmetry broken, the scalar component of superfields \hat{H}_u , \hat{H}_d and \hat{S} can be written as

$$H_u = \begin{pmatrix} H_u^+ \\ v_u + \frac{H_u^R + iH_u^I}{\sqrt{2}} \end{pmatrix}, \quad H_d = \begin{pmatrix} v_d + \frac{H_d^R + iH_d^I}{\sqrt{2}} \\ H_d^- \end{pmatrix}, \quad S = v_s + \frac{S^R + iS^I}{\sqrt{2}}, \quad (2.5)$$

where H_u^R, H_d^R , and S^R are CP-even component fields, H_u^I, H_d^I , and S^I are the CP-odd component fields, and the H_u^+ and H_d^- are charged component fields. In practice, it is convenient to rotate the fields as

$$H_1 = \cos\beta H_u + \varepsilon \sin\beta H_d^* = \begin{pmatrix} H^+ \\ \frac{S_1 + iP_1}{\sqrt{2}} \end{pmatrix} \quad (2.6)$$

$$H_2 = \sin\beta H_u - \varepsilon \cos\beta H_d^* = \begin{pmatrix} G^+ \\ v + \frac{S_2 + iG^0}{\sqrt{2}} \end{pmatrix} \quad (2.7)$$

$$H_3 = S = v_s + \frac{S_3 + iP_2}{\sqrt{2}} \quad (2.8)$$

where $\varepsilon = \begin{pmatrix} 0 & 1 \\ -1 & 0 \end{pmatrix}$, and H_2 , H_1 and H_3 are the SM Higgs doublet, new doublet and singlet respectively.

In the basis (S_1, S_2, S_3) , the CP-even Higgs boson mass matrix M_S^2 is given by [45, 46]

$$M_{S,11}^2 = M_A^2 + (m_Z^2 - \lambda^2 v^2) \sin^2 2\beta + \Delta M_{S,11}^2, \quad (2.9)$$

$$M_{S,22}^2 = m_Z^2 \cos^2 2\beta + \lambda^2 v^2 \sin^2 2\beta + \Delta M_{S,22}^2, \quad (2.10)$$

$$M_{S,12}^2 = -\frac{1}{2} (m_Z^2 - \lambda^2 v^2) \sin 4\beta + \Delta M_{S,12}^2, \quad (2.11)$$

$$M_{S,33}^2 = \frac{1}{4} \lambda^2 v^2 \left(\frac{M_A}{\mu / \sin 2\beta} \right)^2 + \kappa v_s A_\kappa + 4(\kappa v_s)^2 - \frac{1}{2} \lambda \kappa v^2 \sin 2\beta, \quad (2.12)$$

$$M_{S,13}^2 = - \left(\frac{M_A^2}{2\mu / \sin 2\beta} + \kappa v_s \right) \lambda v \cos 2\beta, \quad (2.13)$$

$$M_{S,23}^2 = 2\lambda \mu v \left[1 - \left(\frac{M_A}{2\mu / \sin 2\beta} \right)^2 - \frac{\kappa}{2\lambda} \sin 2\beta \right], \quad (2.14)$$

where M_A is the mass scale of new doublet with

$$M_A^2 = \frac{2\mu(A_\lambda + \kappa v_s)}{\sin 2\beta}, \quad (2.15)$$

and $\Delta M_{S,11}^2$, $\Delta M_{S,22}^2$ and $\Delta M_{S,12}^2$ are the important corrections at loop level. The first-order contributions by stop loops are given by [46]

$$\Delta M_{S,11}^2 = \frac{3v^2 y_t^4 \sin^2 2\beta}{32\pi^2} \left[\ln \left(\frac{M_S^2}{m_t^2} \right) + \frac{X_t Y_t}{M_S^2} \left(1 - \frac{X_t Y_t}{12M_S^2} \right) \right], \quad (2.16)$$

$$\Delta M_{S,22}^2 = \frac{3v^2 y_t^4 \sin^4 \beta}{8\pi^2} \left[\ln \left(\frac{M_S^2}{m_t^2} \right) + \frac{X_t^2}{M_S^2} \left(1 - \frac{X_t^2}{12M_S^2} \right) \right], \quad (2.17)$$

$$\Delta M_{S,12}^2 = \frac{3v^2 y_t^4 \sin^2 \beta \sin 2\beta}{16\pi^2} \left[\ln \left(\frac{M_S^2}{m_t^2} \right) + \frac{X_t(X_t + Y_t)}{2M_S^2} - \frac{X_t^3 Y_t}{12M_S^2} \right], \quad (2.18)$$

where $X_t = A_t - \mu / \tan \beta$, $Y_t = A_t + \mu \tan \beta$, $M_S = \sqrt{m_{t_1} m_{t_2}}$ is the geometric average of the two stop masses and A_t is the trilinear parameter associated with the Yukawa coupling of top quark $y_t = m_t / v$. To have the SM-like Higgs at about 125 GeV, with $\tan \beta \gg 1$ and $\lambda \ll 1$ the loop correction $\Delta M_{S,22}$ need to be about $(86 \text{ GeV})^2$, which means heavy stops ($M_S \sim 10 \text{ TeV}$), or large stop mixing parameter A_t .

In the basis (P_1, P_2) , the CP-odd Higgs boson mass matrix M_P^2 is

$$M_{P,11}^2 = M_A^2, \quad (2.19)$$

$$M_{P,12}^2 = \lambda v (A_\lambda - 2\kappa v_s), \quad (2.20)$$

$$M_{P,22}^2 = \lambda (A_\lambda + 4\kappa v_s) \frac{v_u v_d}{v_s} - 3\kappa v_s A_\kappa. \quad (2.21)$$

Three CP-even mass eigenstates h_i ($i = 1, 2, 3$) (ordered in mass) are mixed from S_i ($i = 1, 2, 3$), and two CP-odd mass eigenstates a_i ($i = 1, 2$) (ordered in mass) are mixed from P_i ($i = 1, 2$). The mixings are given by

$$\begin{pmatrix} h_1 \\ h_2 \\ h_3 \end{pmatrix} = S_{ij} \begin{pmatrix} S_1 \\ S_2 \\ S_3 \end{pmatrix}, \quad \begin{pmatrix} a_1 \\ a_2 \end{pmatrix} = P_{ij} \begin{pmatrix} P_1 \\ P_2 \end{pmatrix}, \quad (2.22)$$

where the mixing matrix S_{ij} and P_{ij} can diagonalize the mass matrix M_S^2 and M_P^2 respectively.

The neutralino sector consists of five neutralinos. In the gauge-eigenstate basis $\psi^0 = (\tilde{B}, \tilde{W}^3, \tilde{H}_d^0, \tilde{H}_u^0, \tilde{S})$, the neutralino mass matrix takes the form [47]

$$M_{\tilde{\chi}^0} = \begin{pmatrix} M_1 & 0 & -c_\beta s_W m_Z & s_\beta s_W m_Z & 0 \\ 0 & M_2 & c_\beta c_W m_Z & -s_\beta c_W m_Z & 0 \\ -c_\beta s_W m_Z & c_\beta c_W m_Z & 0 & -\mu & -\lambda v_d \\ s_\beta s_W m_Z & -s_\beta c_W m_Z & -\mu & 0 & -\lambda v_u \\ 0 & 0 & -\lambda v_d & -\lambda v_u & 2\kappa v_s \end{pmatrix} \quad (2.23)$$

where $s_\beta = \sin \beta$, $c_\beta = \cos \beta$, $s_W = \sin \theta_W$, $c_W = \cos \theta_W$. The mass eigenstates are denoted by $\tilde{\chi}_i^0$ ($i = 1, 2, 3, 4, 5$) ordered in mass. Hereinafter $\tilde{\chi}_1^0$ is identified as the LSP.

Combining with Eq.(2.12), Eq.(2.21) and Eq.(2.23), we get a relation [30, 48] :

$$M_{\tilde{\chi}^0, 55}^2 = 4\kappa^2 v_s^2 = M_{S, 33}^2 + \frac{1}{3} M_{P, 22}^2 - \frac{4}{3} v_u v_d \left(\frac{\lambda^2 A_\lambda}{\mu} + \kappa \right). \quad (2.24)$$

If the LSP $\tilde{\chi}_1^0$ is highly singlino-dominated, h_1 and a_1 are singlet-dominated, and with a sizable $\tan \beta$, a not-too-large A_λ , and small λ and κ , this equation can become:

$$m_{\tilde{\chi}_1^0}^2 \approx m_{h_1}^2 + \frac{1}{3} m_{a_1}^2. \quad (2.25)$$

2.2 The Heuristically Search (HS)

Usually, We divide the samples into 2 categories according to whether or not the samples passed all constraints. A sample that violated several constraints might be not good enough, but there is a chance that we can lead it to become a good sample.

In our case, we first leave aside the dark matter and muon g-2 constraints, only imposing other constraints in the **NMSSMTools**. A sample that passes other constraints will get a score to evaluate how much it violates the dark matter and muon g-2 constraints, and we call it a ‘**marginal sample**’.

Table 1. The three types of samples: the bad, marginal and perfect samples.

	Type 1	Type 2	Type 3
The basic constraints	×	✓	✓
The dark matter and muon g-2 constraints	—	×	✓
	bad samples	marginal samples	perfect samples
Score	None	>0	=0

In Table 1, we classify the samples into 3 types: the bad, marginal and perfect samples. For marginal and perfect samples, they will get a score to value how much they violate the

constraints. And we try to shift these marginal samples to satisfy the dark matter and muon g-2 constraints, becoming perfect samples. The score function is given as:

$$f(\mathbf{X}) = \sum_{i=1}^N \max \left[1 - \frac{O_{\text{Theor.max}}^i}{O_{\text{Exp.min}}^i}, 0 \right] + \max \left[\frac{O_{\text{Theor.min}}^i}{O_{\text{Exp.max}}^i} - 1, 0 \right], \quad (2.26)$$

where \mathbf{X} represent a marginal sample, O^i means the i -th observable depending on \mathbf{X} , the N means there are N kinds of different observables, the $O_{\text{Theor.min}}^i$ and $O_{\text{Theor.max}}^i$ are calculated with NMSSMTools, and the $O_{\text{Exp.min}}^i$ and $O_{\text{Exp.max}}^i$ are given by experimental results. When the score is large, it means the marginal sample violates the experiments more; while when the score is zero, it means the marginal sample becomes a perfect sample, and satisfies all constraints very well, including dark matter and muon g-2 constraints.

In Algorithm 1, we give the **Heuristically Search algorithm**, which can shift a marginal sample to a perfect sample satisfying all constraints. With a marginal sample, \mathbf{X} , we search around it and try to find another marginal sample with a smaller score. Then we repeat the process, until we meet a perfect sample whose score is zero, or get failed.

Algorithm 1 The Heuristically Search (HS) with NMSSMTools

Input: A marginal sample, \mathbf{X} ;

Output: Find a perfect sample \mathbf{X} passed all constraints, or failed;

```

1: initial  $step = 0$  and  $try = 0$ 
2:  $score \leftarrow f(\mathbf{X})$ 
3: while  $step < N_{max}$  and  $try < T_{max}$  and  $score \neq 0$  do
4:   get a new marginal sample  $\mathbf{X}'$  around the  $\mathbf{X}$  within radius  $r$ 
5:    $score' \leftarrow f(\mathbf{X}')$ 
6:   if  $score' < score$  then
7:      $\mathbf{X} \leftarrow \mathbf{X}'$ 
8:      $score \leftarrow score'$ 
9:      $step \leftarrow step + 1$ 
10:     $try \leftarrow 0$ 
11:   else
12:      $try \leftarrow try + 1$ 
13:   end if
14:   // the search radius  $r$  can be change with different  $score$ 
15: end while
16: if  $score = 0$  then
17:   Succeed in getting a perfect sample  $\mathbf{X}$ 
18: else
19:   Failed
20: end if
```

The search can be successful or get failed. Most of the time in our case, the Heuristically Search can lead about 80% (even over 94%) marginal samples to perfect samples. Meanwhile, to avoid the program being trapped in a local minimum, we give it a chance to

give up. During the search, if the search step is larger than the maximum step N_{\max} (we set it to 20), or the number of tries in one step is larger than the maximum number, T_{\max} (we set it to 50), we stop the program and the search gets failed.

To get a new marginal sample \mathbf{X}' around the \mathbf{X} , we can treat each component \mathbf{x}_i ($i = 1 \dots 9$) independently. The simplest way is choosing samples around the \mathbf{x}_i within radius r_i with uniform distribution. To improve the efficiency, the Gaussian distribution is adopted, since it has some chance to search samples far away and could jump out of the local minimums. The Gaussian distribution function of \mathbf{x}'_i is given as:

$$f(\mathbf{x}'_i) = \frac{1}{\sqrt{2\pi}\sigma_i} \exp \left[-\frac{(x'_i - x_i)^2}{2\sigma_i^2} \right], \quad (2.27)$$

$$\sigma_i = r_i(x_{i,\max} - x_{i,\min}), \quad (2.28)$$

where r_i (we set it to 1/50) is an important parameter and determines the search efficient. Actually, r_i can change with the score. When the score is nearly zero, it means that a perfect sample is nearby, and then r_i can change to a smaller one and vice versa.

2.3 The Generative Adversarial Network (GAN)

The Generative Adversarial Network (GAN) is a Generative model. It can generate samples with similar distribution as the real data. There are two neural networks in GAN. One is the Generator \mathbf{G} , which can generate fake samples. While the other is the Discriminator \mathbf{D} , which can classify the generated samples into real samples and the fake samples, so it is actually a binary classifier.

When the GAN is being trained, the Discriminator \mathbf{D} tries to classify the generated samples into real and fake samples, meanwhile the Generator \mathbf{G} tries to fool the Discriminator \mathbf{D} and generate almost ‘real’ samples. After training, the Generator \mathbf{G} and Discriminator \mathbf{D} arrive at a Nash equilibrium. Then we can use the Generator \mathbf{G} to generate ‘real’ samples as many as we need. And these ‘real’ samples actually have similar distribution as the real samples coming from the training dataset.

In this work, we use the Artificial Neural Networks to build the Generator \mathbf{G} and the Discriminator \mathbf{D} . We adopt a simple Neural Network with 3 hidden layers and each layer with 50 neurons, and the Activation Function is Leaky ReLU. Furthermore, we train our GAN with Algorithm 2. In our case, we choose $k = 3$, $n = 1$, $m = 20000$, and the training iterations as 2000, while for the Gradient descent we use Adadelta [49].

During the training, we require the Generator to learn the general distribution of the real data, but not try hard to find perfect hyperparameters, since we need the Generator to have more creativity. As a complement, we combine GAN with the HS. The Generator generates lots of samples, and some of them might be marginal samples, while the HS program will try to lead these marginal samples to perfect samples.

3 Results and discussions

To satisfy all the constraints including muon g-2, dark matter, Higgs data, gluino and other SUSY search results, and try to get right dark matter relic density and large Higgs invisible

Algorithm 2 Training the Generative Adversarial Network (GAN)

```
1: for number of training iterations do
2:   for  $k$  steps training the Discriminator do
3:     get  $m$  perfect samples  $\{\mathbf{X}^{(1)}, \dots, \mathbf{X}^{(m)}\}$ , from the training dataset;
4:     get  $m$  noise samples,  $\{\mathbf{z}^{(1)}, \dots, \mathbf{z}^{(m)}\}$ , generated by the Generator;
5:     update the Discriminator by descending its binary cross entropy
6:   end for
7:   for  $n$  steps training the Generator do
8:     get  $m$  noise sample,  $\{\mathbf{z}^{(1)}, \dots, \mathbf{z}^{(m)}\}$ , generated by the Generator
9:     update the Generator by descending its binary cross entropy
10:  end for
11: end for
```

decay, we consider following parameter space in the scNMSSM:

$$\begin{aligned} 0.1 < \mu < 0.2 \text{ TeV}, \quad 0 < M_0 < 0.5 \text{ TeV}, \quad 0.5 < M_{1/2} < 2 \text{ TeV}, \\ 0.0 < \lambda < 0.7, \quad |\kappa| < 0.7, \quad 1 < \tan \beta < 30, \\ |A_0| < 10 \text{ TeV}, \quad |A_\lambda| < 10 \text{ TeV}, \quad |A_\kappa| < 10 \text{ TeV}. \end{aligned} \quad (3.1)$$

3.1 Scan with HS and GAN

We developed the Heuristically Search program based on NMSSMTools-5.5.2 [50–53]. During the scan, we first require the samples satisfying the following other basic constraints:

- Theoretical constraints of vacuum stability, and without Landau pole below M_{GUT} [50–52].
- The lower mass bounds of charginos and sleptons from the LEP:

$$m_{\tilde{\tau}} \geq 93.2 \text{ GeV}, \quad m_{\tilde{\chi}_1^\pm} \geq 103.5 \text{ GeV} \quad (3.2)$$

- Constraints from B physics, such as $B_s \rightarrow \mu^+ \mu^-$, $B_d \rightarrow \mu^+ \mu^-$, $b \rightarrow s \gamma$ and the mass differences Δm_d , Δm_s [54–57]

$$1.7 \times 10^{-9} < Br(B_s \rightarrow \mu^+ \mu^-) < 4.5 \times 10^{-9} \quad (3.3)$$

$$1.1 \times 10^{-10} < Br(B_d \rightarrow \mu^+ \mu^-) < 7.1 \times 10^{-10} \quad (3.4)$$

$$2.99 \times 10^{-4} < Br(b \rightarrow s \gamma) < 3.87 \times 10^{-4} \quad (3.5)$$

- An SM-like Higgs boson exists with a mass between $123 \sim 127 \text{ GeV}$, and satisfies the global fit results with Higgs data at Run I and Run II of the LHC [3, 58, 59].
- To study Higgs invisible decay we require the mass of $\tilde{\chi}_1^0$ lighter than half of the SM-like Higgs,

$$m_{\tilde{\chi}_1^0} < \frac{1}{2} m_{h_{\text{SM}}} \quad (3.6)$$

Table 2. The upper and lower bounds of the dark matter and muon g-2 observables.

	lower limit	upper limit
The DM relic density Ωh^2	None	0.131
The spin-independent DM-nucleon cross section	None	XENON1T
The spin-dependent DM-neutron cross section	None	LUX and XENON1T
The spin-dependent DM-proton cross section	None	LUX, XENON1T and PICO-60
Muon g-2 δa_μ	8.8×10^{-10}	46×10^{-10}

Then for the marginal samples, we consider the constraints of dark matter and muon g-2, calculating the score in Eq.(2.26) for each sample. The upper and lower bounds of these observables are given in Table.2. The detail experimental constraints we consider in this work are list as following:

- The DM relic density Ωh^2 from WMAP/Planck [54, 60, 61], we only take upper bound $\Omega h^2 \leq 0.131$, considering there may be other sources of DM that contribute to Ωh^2 ; where the dark matter observables are calculated by micrOMEGAs 5.0 [62–65] inside NMSSMTools.
- The spin-independent DM-nucleon cross section is constrained by XENON1T [66], where we rescale the original values by Ω/Ω_0 with $\Omega_0 h^2 = 0.1187$;
- The spin-dependent DM-nucleon cross section is constrained by LUX [67], XENON1T [68] and PICO-60 [69], where we also rescale the original values by Ω/Ω_0 ;
- The muon anomalous magnetic moment (muon g-2) is constrained at 2σ level including all errors. The difference between experimental result and SM theoretical value, including the corresponding error is given by [70–74]

$$\delta a_\mu \equiv a_\mu^{\text{ex}} - a_\mu^{\text{SM}} = (27.4 \pm 9.3) \times 10^{-10} \quad (3.7)$$

where a_μ^{SM} contains no Higgs contribution, since we consider a SM-like Higgs in SUSY contribution to δa_μ . We also consider the theoretical error of SUSY contribution, which is about 1.5×10^{-10} . Thus at 2σ level, the central value of SUSY (including Higgses) contribution to muon g-2, δa_μ , can be $5.8 \sim 49.0 \times 10^{-10}$.

If a sample satisfies the basic constraints (not including DM and muon g-2), it will get a score as a marginal or perfect sample; otherwise, it will be discarded. Then with the HS program, we did our first scan. We randomly searched for marginal samples in the parameter space, and then used the HS program changing them into perfect samples. In the first search, we got about 10k perfect samples in 24 hours ². In fact if we changed the

²We used 40 threads parallel runing on Intel(R) Xeon(R) CPU E7-4830 v3 @ 2.10GHz.

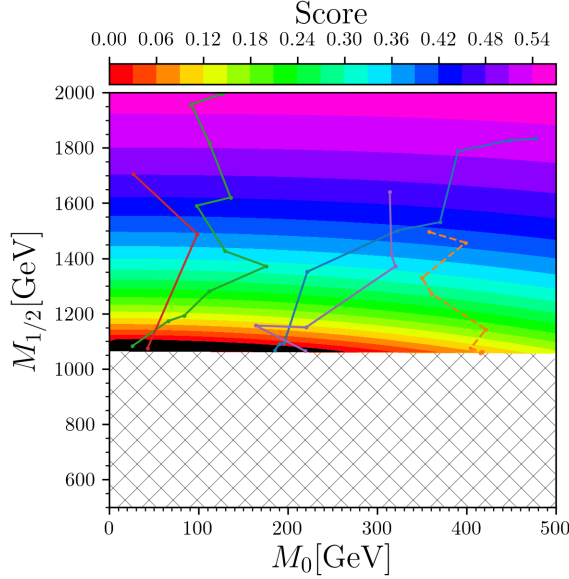


Figure 1. The samples with seven parameters fixed ($\lambda = 0.278$, $\kappa = -0.0577$, $\tan\beta = 17$, $\mu = 162$ GeV, $A_0 = -1924$ GeV, $A_\lambda = 2756$ GeV, and $A_\kappa = 589$ GeV) are projected in the M_0 versus $M_{1/2}$ plane. The colored area indicate where the samples are marginal samples, and the colors indicate their score. The black area indicate where the samples are perfect samples with zero score. While the grid area indicate this piece of parameter space is excluded by the basic constraints. The four solid lines indicate the marginal samples are led to become perfect samples, whereas the dash line indicates that the marginal sample is failed to shift to a perfect sample.

random scan into a multi-path Markov Chain Monte Carlo (MCMC) scan, the scan would be more efficient.

In Fig.1, we show the score of marginal samples in the M_0 versus $M_{1/2}$ plane. Notice that if the score equal to zero, the marginal sample is also a perfect sample. We can see that the area of marginal samples (colored range) is much larger than the perfect samples (black range) which get a zero score (satisfying all above constraints, including the DM and muon g-2). Besides we also show five tries, that the HS program tries to shift marginal samples to perfect samples, where four get success (solid lines) and one gets failure (dashed line). As the successful tries shown, the Heuristically Search usually needs less than 10 steps to shift a marginal sample to a perfect sample. In fact, many marginal samples need only several steps to change into perfect samples, while the direct search for perfect samples will waste much more time. That is the reason why we developed the HS program.

After the first search, all of the 10k perfect samples are used as the training set for the GAN. Then we trained the GAN according to Algorithm 2. With a well-trained GAN ³, we can transform random noises to recommended samples that have similar distribution as the training data. Then we can easily get millions of recommended samples from the GAN in a few seconds.

In Fig.2, we show the training set in the upper panels, and the recommended samples

³We used Pytorch v1.3 to develop the GAN, and training cost about 5 hours. CPU: I5 6600K, GPU: GTX 1660 super.

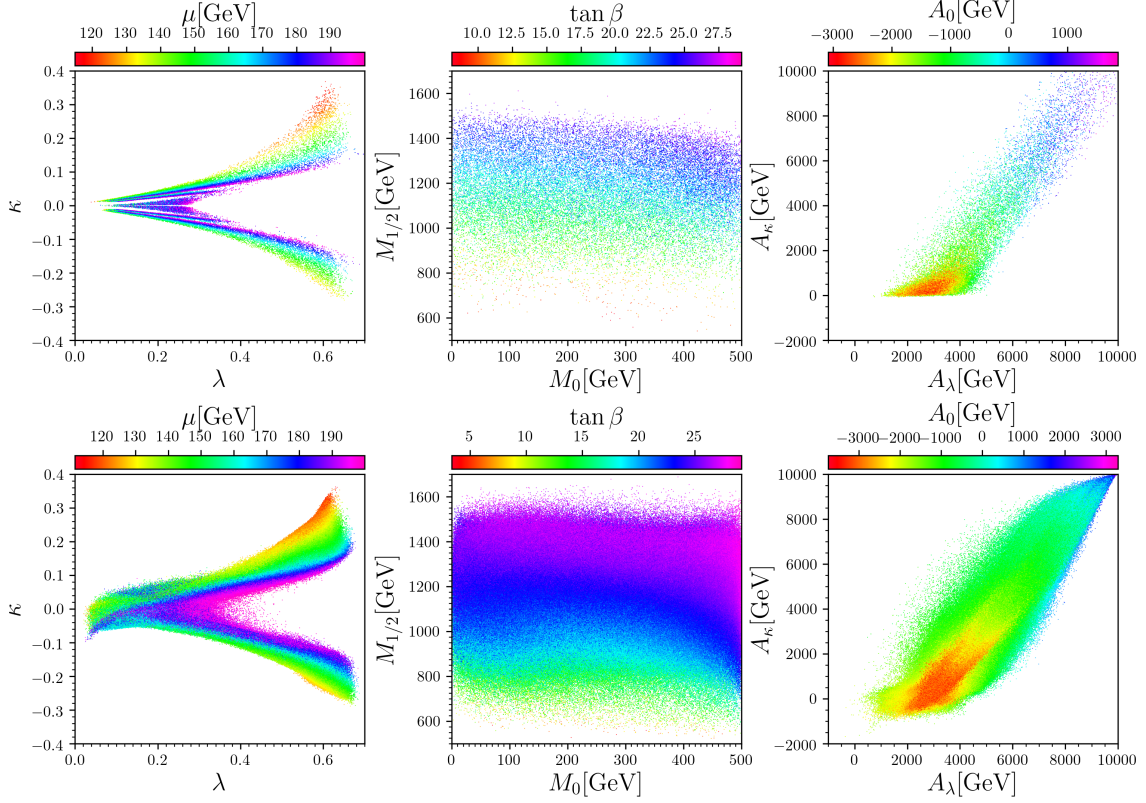


Figure 2. The samples' distributions in the κ versus λ (left), $M_{1/2}$ versus M_0 (middle), A_κ versus A_λ (right) planes. From left to the right, colors indicate the μ , $\tan\beta$ and A_0 , respectively. **Upper Panel:** The training set for GAN, which are the original perfect samples generated in our first search. **Lower Panel:** The recommended samples from GAN, which are generated by the Generator **G** in our well-trained GAN.

from GAN in the lower panels. We can see that the GAN has already learned the general distribution of the perfect samples in the training set. While the recommended samples from GAN (in the lower panels) have some creativity, which is not totally identical to the training set (in the upper panels). The well-trained GAN can exploit the parameter space and recommend samples around the training samples, which is exactly what we need.

We used the trained GAN to generate 2000k recommended samples⁴, and passed these recommended samples to the HS program. Then we got 280k perfect samples within 30 hours⁵, such a way is much faster than the traditional parameter scan. At last, we impose the following additional constraints:

- The upper limit of Higgs invisible decay, 19%, given by the CMS collaboration [7].
- The lower mass bound of colored sparticles,

$$m_{\tilde{g}} > 2 \text{ TeV}, m_{\tilde{t}_1} > 0.7 \text{ TeV}, m_{\tilde{q}_{1,2}} > 2 \text{ TeV}. \quad (3.8)$$

⁴Less than 1 minute on the computer with CPU: I5 6600K, GPU: GTX 1660 super.

⁵We used 40 threads parallel running on Intel(R) Xeon(R) CPU E7-4830 v3 @ 2.10GHz.

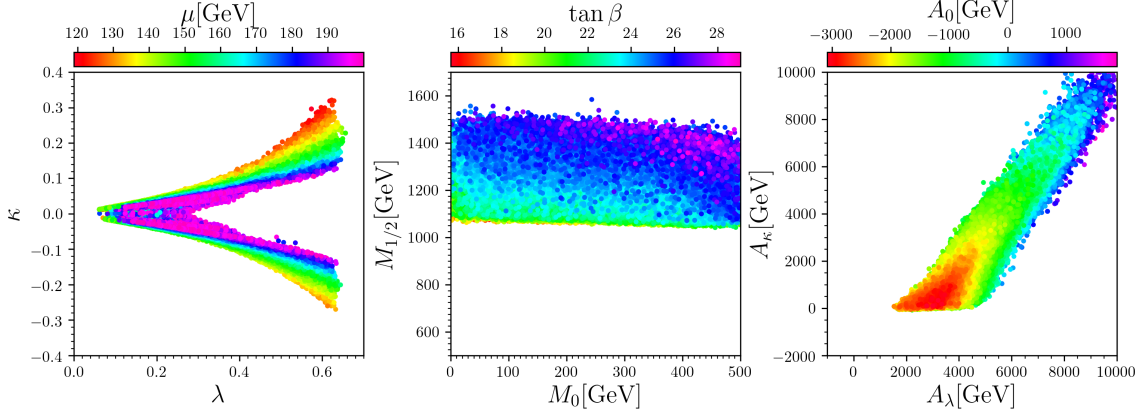


Figure 3. The final surviving samples in the κ versus λ (left), $M_{1/2}$ versus M_0 (middle), A_κ versus A_λ (right) planes. From left to the right, colors indicate the μ , $\tan\beta$ and A_0 , respectively.

- The CMS constraints on charginos and neutralinos [75] implemented inside NMSSMTools-5.5.2.
- The SUSY search results implemented inside SModelS v1.2.2 [76–82] with official 1.2.2 database.
- The low- and high-mass resonances search results at the LEP, Tevatron and LHC, which are implemented inside HiggsBounds-5.5.0 [83–87].

Finally, after all the scans and constraints, we got about 88k surviving samples. In Fig.3, we show the nine free parameters of these surviving samples, and the coordinates are the same as those in Fig.2. We can see that all $M_{1/2}$ are larger than 1200 GeV. The reason is that we imposed the additional constraints, especially the high mass bound of gluino and the first-two-generation squarks at the LHC in Eq.(3.8).

Comparing Fig.3 with the lower panels in Fig.2, we can see that the recommended samples from GAN are changed to perfect samples by HS program. While comparing Fig.3 with the upper plane in Fig.2, we can see that the GAN has recommended many marginal samples that we need, and it does have some creativity to recommend samples around the training samples. So, the combination of HS and GAN is very crucial.

3.2 Light dark matter (DM) and Higgs invisible decay

In Fig.4 we show the final surviving samples in the plane of κ vs λ , with colors indicate the masses of the lightest neutralino $\tilde{\chi}_1^0$, the lightest CP-even Higgs h_1 and the light CP-odd Higgs a_1 respectively. For the surviving samples, we checked that the lightest CP-even Higgs h_1 are all highly singlet-dominated, and the next-to-lightest CP-even Higgs h_2 is the SM-like Higgs of 125 GeV. Since we need the SM-like Higgs have a chance decaying to invisible $\tilde{\chi}_1^0$, the $\tilde{\chi}_1^0$ is lighter than $m_{h_2}/2$. If the LSP $\tilde{\chi}_1^0$ is singlino-dominated, according Eq.(2.23), we should have

$$m_{\tilde{\chi}_1^0} = 2\kappa v_s = 2\frac{\kappa}{\lambda}\mu \leq m_{h_2}/2. \quad (3.9)$$

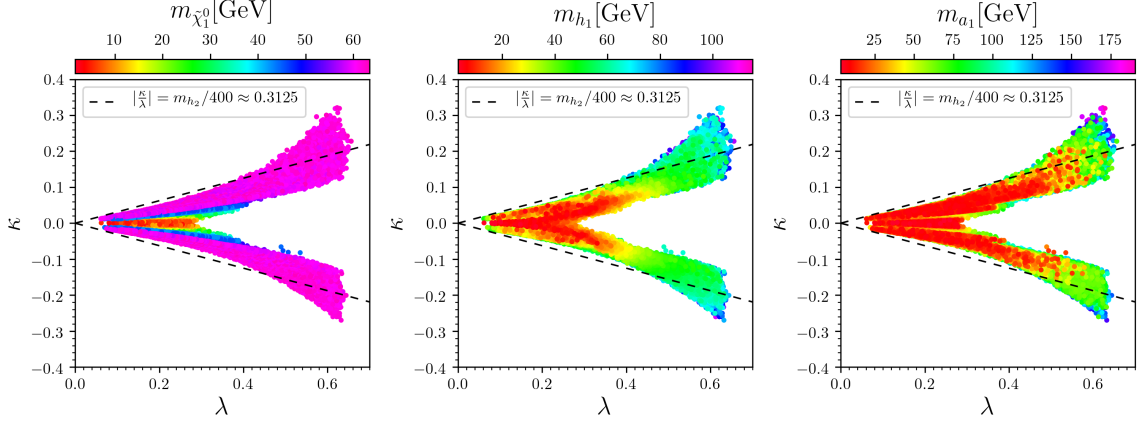


Figure 4. The final surviving samples in the κ versus λ planes. From left to the right, colors indicate the lightest neutralino (LSP) mass $m_{\tilde{\chi}_1^0}$, the lightest CP-even Higgs h_1 mass m_{h_1} and the light CP-odd Higgs a_1 mass m_{a_1} , respectively. The dash line is $\left|\frac{\kappa}{\lambda}\right| = 125/400 \approx 0.3125$. In all these planes, samples with smaller mass are projected on top of the larger ones.

Since we set the parameter μ from 100 to 200 GeV, we have

$$\left[\frac{\kappa}{\lambda}\right]_{\max} \leq \left[\frac{m_{h_2}}{4\mu}\right]_{\min} = \frac{m_{h_2}}{4 \times 100} \approx 0.3125. \quad (3.10)$$

Thus it is and we checked that the $\tilde{\chi}_1^0$ are singlino-dominated for samples between the two dash line. We can also see that for the samples between the two dash lines, h_1 and a_1 are also possibly lighter than $m_{h_2}/2$.

In Fig.5 we show the properties of dark matter in the scNMSSM. In the lower panels, the spin-independent dark matter and nucleon scattering cross section σ_{SI} have been rescaled by a ratio of Ω/Ω_0 , where the Ω_0 is the right dark matter relic density with $\Omega_0 h^2 = 0.1187$. As seen from these panels, the samples with right relic density can be divided into three cases:

- **Case I:** $m_{\tilde{\chi}_1^0} \simeq m_{h_2}/2$
- **Case II:** $m_{\tilde{\chi}_1^0} \simeq m_Z/2$
- **Case III:** $m_{\tilde{\chi}_1^0} \lesssim 12 \text{ GeV}$

From Fig.5, we can obtain the following observations:

- From the upper left panel, the samples with right DM relic density are all with highly singlino-dominated $\tilde{\chi}_1^0$, where $|N_{15}|^2 \gtrsim 0.9$.
- From the upper right panel, there is a special relationship between the mass of h_1 , a_1 and $\tilde{\chi}_1^0$. For the samples with right DM relic density in Case I and Case II, the LSP $\tilde{\chi}_1^0$ is highly singlino-dominated, and with small λ , κ and a sizable $\tan\beta$. Combining

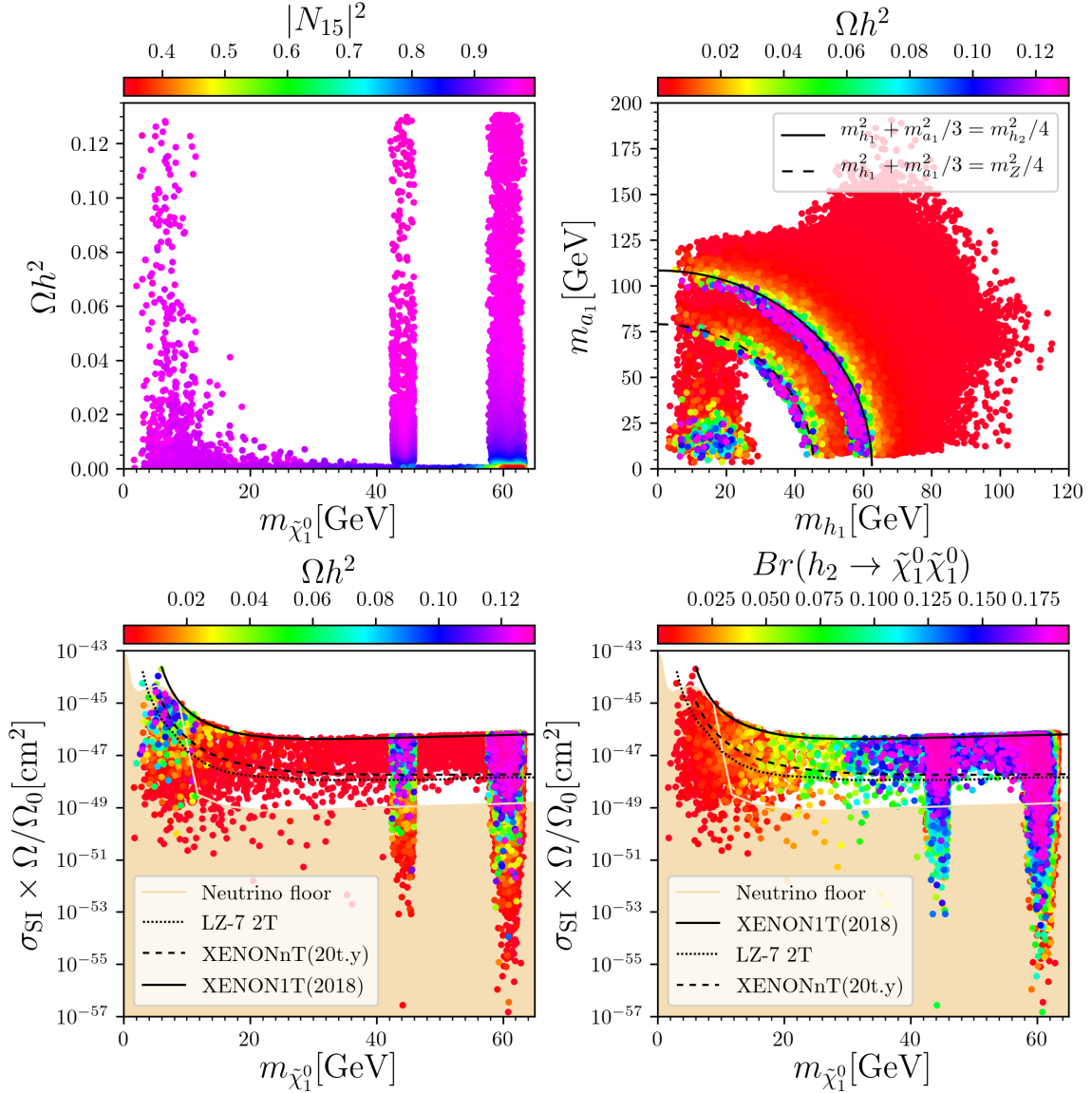


Figure 5. **Upper Panel:** The surviving samples in the DM relic density Ωh^2 versus the lightest neutralino (LSP) mass $m_{\tilde{\chi}_1^0}$ (left), and the CP-odd Higgs mass m_{a_1} versus the CP-even Higgs mass m_{h_1} (right) planes. Colors indicate the singlino component $|N_{15}|^2$ in the $\tilde{\chi}_1^0$ (left), and the DM relic density Ωh^2 (right) respectively. In the right panel, the black solid and dashed curves indicate $m_{h_1}^2 + m_{a_1}^2/3 = m_{h_2}^2/4$ and $m_{h_1}^2 + m_{a_1}^2/3 = m_Z^2/4$ respectively. Samples with larger $|N_{15}|^2$ (left) or Ωh^2 (right) are projected on top of the smaller ones. **Lower Panel:** The surviving samples in the spin-independent DM-nucleon scattering cross section ($\sigma_{\text{SI}} \times \Omega/\Omega_0$) versus the LSP mass $m_{\tilde{\chi}_1^0}$ planes. Colors indicate the DM relic density Ωh^2 (left), and the Higgs invisible decay $Br(h_2 \rightarrow \tilde{\chi}_1^0 \tilde{\chi}_1^0)$ (right) respectively. In these two panels, the black solid, dashed and dotted curves indicate the limits of spin-independent DM-nucleon cross section σ_{SI} by XENON1T 2018 [66], the future detection sensitivity of XENONnT and LUX-ZEPLIN (LZ-7 2T), and the orange shaded region indicate the neutrino floor [88]. Samples with larger Ωh^2 (left) or $Br(h_2 \rightarrow \tilde{\chi}_1^0 \tilde{\chi}_1^0)$ (right) are projected on top of the smaller ones.

with Eq.(2.25), we can see the two ellipse arcs:

$$\text{Case I : } m_{h_1}^2 + \frac{1}{3}m_{a_1}^2 \simeq m_{\tilde{\chi}_1^0}^2 \simeq \left(\frac{m_{h_2}}{2}\right)^2 \quad (3.11)$$

$$\text{Case II : } m_{h_1}^2 + \frac{1}{3}m_{a_1}^2 \simeq m_{\tilde{\chi}_1^0}^2 \simeq \left(\frac{m_Z}{2}\right)^2 \quad (3.12)$$

- From the lower-left panel, most samples predict spin-independent DM-nucleon cross section σ_{SI} not far below the bound from XENON1T 2018, and can be covered by future LZ and XENONnT experiments. Thus these two future direct detections are crucial to check the parameter space of the scNMMSM. But there are still some samples that can escape from these future detections, and also can predict right relic density. Besides, there are also some samples below the neutrino floor, although most of them do not predict sufficient DM relic density.
- From the lower right panel, samples with large Higgs invisible decay branching ratio, $Br(h_2 \rightarrow \tilde{\chi}_1^0 \tilde{\chi}_1^0) > 10\%$, have a sizable LSP mass, $m_{\tilde{\chi}_1^0} > 30$ GeV. This is because the small LSP mass, $m_{\tilde{\chi}_1^0} < 30$ GeV, always accompanying with a small h_1 and a_1 mass, which can be seen from the upper right panel of Fig.4. Then the exotic decay channels $h_2 \rightarrow h_1 h_1$ and $h_2 \rightarrow a_1 a_1$ will open, which can be seen in Fig.6. The Higgs invisible decay branching ratio $Br(h_2 \rightarrow \tilde{\chi}_1^0 \tilde{\chi}_1^0)$ become smaller.
- From the lower right panel, most samples which have large Higgs invisible decay branching ratio, $Br(h_2 \rightarrow \tilde{\chi}_1^0 \tilde{\chi}_1^0) > 10\%$, could be covered by future LZ and XENONnT detections. But there are still some samples that can escape from these future experiments, and also can have large Higgs invisible decay branching ratio. And there are also some samples below the neutrino floor, some of them can have large Higgs invisible decay branching ratio $Br(h_2 \rightarrow \tilde{\chi}_1^0 \tilde{\chi}_1^0) > 10\%$.

In Fig.6, we show the decay information of the SM-like Higgs h_2 . From this figure, we can see that all of the branching ratios of $h_2 \rightarrow \tilde{\chi}_1^0 \tilde{\chi}_1^0, h_1 h_1, a_1 a_1$ can be at most about 20%. While we checked that considering in addition that of h_2 decay to $4\tilde{\chi}_1^0$ though $a_1/h_1 \rightarrow \tilde{\chi}_1^0 \tilde{\chi}_1^0$, which acquire $m_{\tilde{\chi}_1^0} < m_{h_2}/4 \simeq 31$ GeV, the branching ratio of Higgs invisible decay increase very little compared with only that h_2 decay to two $\tilde{\chi}_1^0$ though $h_2 \rightarrow \tilde{\chi}_1^0 \tilde{\chi}_1^0$. The upper limit of Higgs invisible decay branching ratio is about 19% at Run II of the LHC, while the future detections for that can reach to 5.6%, 0.24%, 0.5% and 0.26% according to HL-LHC [89], CEPC [90], FCC [91] and ILC [92] respectively.

Considering the values of $|N_{15}|^2$, we can have the following observations from Fig.6:

- For most samples with higgsino-dominated LSP, $|N_{15}|^2 < 0.5$, the branching ratio $Br(h_2 \rightarrow \tilde{\chi}_1^0 \tilde{\chi}_1^0)$ can be sizeable, while the branching ratio $Br(h_2 \rightarrow h_1 h_1)$ and $Br(h_2 \rightarrow a_1 a_1)$ are both zero. The reason is that the higgsino-dominated LSPs are usually accompanied by a large mass of h_1 and a_1 , as can be seen from the upper panels of Fig.5, thus these two exotic decay channels are closed.
- For samples with h_2/Z -funnel dark matter, $m_{\tilde{\chi}_1^0} \simeq m_{Z, h_2}$, the branching ratio of Higgs boson invisible decay can be large or small depending on the parameter λ .

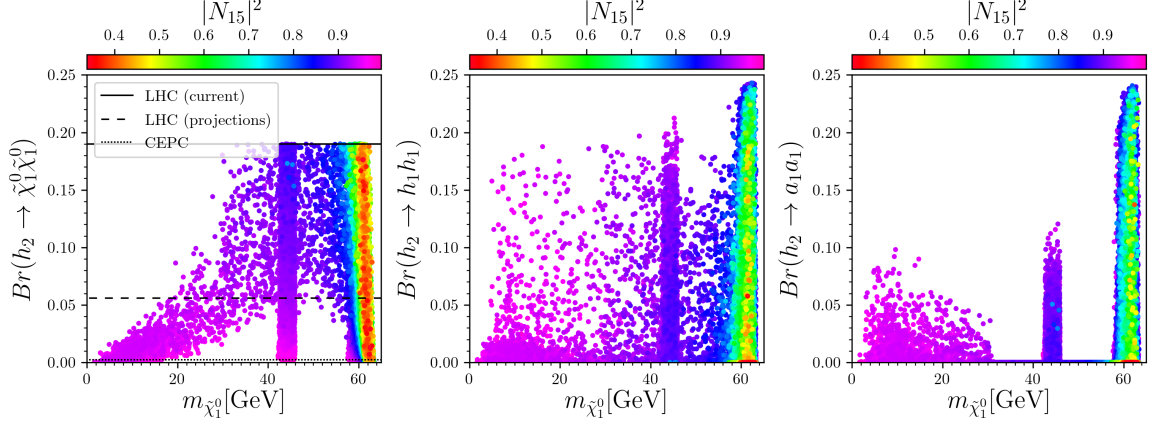


Figure 6. The surviving samples in the Higgs invisible decay $Br(h_2 \rightarrow \tilde{\chi}_1^0 \tilde{\chi}_1^0)$ (left), Higgs exotic $Br(h_2 \rightarrow h_1 h_1)$ (middle) and $Br(h_2 \rightarrow a_1 a_1)$ (right) versus the LSP mass $m_{\tilde{\chi}_1^0}$ planes respectively. Colors indicate the singlino component $|N_{15}|^2$ in the LSP $\tilde{\chi}_1^0$. In the left panel, the black dashed, dash-dotted and dotted lines indicate the Higgs invisible decay upper limit from the current LHC 19% [7], future HL-LHC 5.6% [89], and CEPC 0.24% [90] respectively. Samples with smaller $|N_{15}|^2$ are projected on top of the larger ones.

- For most samples with low-mass LSP, $m_{\tilde{\chi}_1^0} < 20$ GeV, the branching ratio of Higgs boson invisible decay is small and beyond the ability of HL-LHC, while the $Br(h_2 \rightarrow h_1 h_1)$ can be larger than the $Br(h_2 \rightarrow a_1 a_1)$.
- Though the detection of Higgs invisible decay, about half of the surviving samples can be covered at the future HL-LHC, while the future CEPC can cover most.

In addition, we list some discussions on other related topics in this scenario:

- We had performed a work on the annihilating mechanisms of light dark matter in this scenario [93], where we found that all the samples have the LSP in funnel mechanisms. When the LSP is lighter than 20 GeV, it is in h_1 - or a_1 -funnel mechanism, that is $2m_{\tilde{\chi}_1^0} \simeq m_{h_1}$ or $2m_{\tilde{\chi}_1^0} \simeq m_{a_1}$.
- Higgsbounds has been used to constrain heavy Higgs bosons. We also checked that the heavy bosons h_3 and a_2 are at $2.4 \sim 4.8$ TeV, and their branching ratios to τ pairs are 8% at most. The masses are not covered in Ref.[94], and the production rates are much smaller than the upper limits in Ref.[95]. Furthermore, we are ongoing a new work on the heavy Higgs bosons, especially on how to probe them at the future 100-TeV hadronic collider.
- We again checked the spin-dependent cross sections, and show them in Fig.7. As can be seen from it, both the DM-proton and DM-neutron cross sections satisfy the current constraints. When the LSP density Ωh^2 is sufficient, the upper limit is satisfied directly; while when the LSP density Ωh^2 is insufficient considering there may be other source of dark matter, the upper limit is satisfied by rescaling the cross section by a factor Ω/Ω_0 , which is the ratio of LSP $\tilde{\chi}_1^0$ in current dark matter.

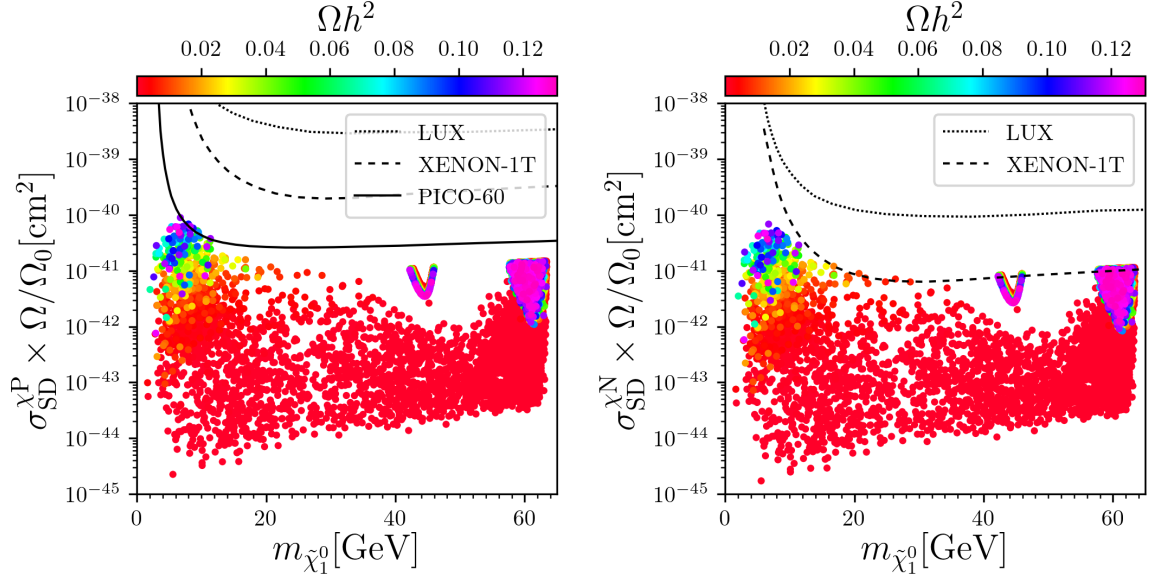


Figure 7. The surviving samples in the spin-dependent cross section of DM-proton scattering $\sigma_{SD}^{\chi^P}$ (left) and DM-neutron scattering $\sigma_{SD}^{\chi^N}$ (right) versus the LSP mass $m_{\tilde{\chi}_1^0}$ planes respectively. Colors indicate the LSP ratio in current dark matter Ω/Ω_0 . In the left panel, the black dotted, dashed and solid curves indicate the limits of spin-dependent DM-proton cross section $\sigma_{SD}^{\chi^P}$ by LUX [67], XENON-1T [68] and PICO-60 [69] respectively. While in the right panel the black dotted and dashed curves indicate these of DM-neutron cross section $\sigma_{SD}^{\chi^N}$ by LUX [67], and XENON-1T [68] respectively. Samples with larger Ωh^2 are projected on top of the smaller ones.

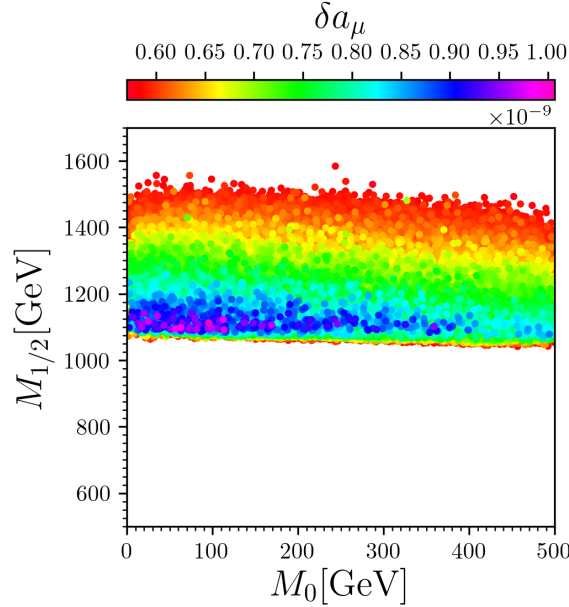


Figure 8. The surviving samples in the parameter $M_{1/2}$ versus M_0 planes, with colors indicating δa_μ , the central value of SUSY (including Higgses) contribution to muon g-2. Samples with larger δa_μ are projected on top of the smaller ones.

- We also checked muon g-2, and show δa_μ , the central value of SUSY (including Higgses) contribution, in Fig.8. When imposing the constraint, we also consider the error in SUSY-contribution calculation, which is about 1.5×10^{-10} , thus all the samples can satisfy the experimental result at 2σ level. We also noticed that, the large $M_{1/2}$ values are caused by the high mass bounds of gluino and squarks in the first two generations, and this in return cause heavy wino-like chargino and bino-like neutralino, thus the SUSY contribution δa_μ cannot increase more.

4 Conclusions

In this work, we develop a novel scan method, combining the Heuristically Search (HS) and the Generative Adversarial Network (GAN). The HS can shift marginal samples to perfect samples, and the GAN can generate recommended samples as many as we need from noise.

In our specific process, we first scan the parameter space randomly with **NMSSMTools** under basic constraints, generating marginal samples; then the HS try to shift the marginal samples to perfect samples satisfying in addition the dark matter and muon g-2 constraints; with these randomly-generated perfect samples, the GAN is trained, and then generates a huge amount of recommended samples in a short time; again the HS try to shift the recommended samples to perfect samples; finally, we check the final perfect samples with additional constraints including these of sparticle searches, Higgs searches and Higgs invisible decay, getting the final surviving samples.

With this efficient method, we find a new scenario in the semi-constrained Next-to Minimal Supersymmetric Standard Model (scNMSSM), or NMSSM with non-universal Higgs masses. In this scenario,

- Both muon g-2 and right relic density can be satisfied, along with the high mass bound of gluino, etc. As far as we know, that had not been realized in the scNMSSM before this work.
- With the right relic density, the lightest neutralinos are singlino-dominated, and can be as light as 0-12 GeV.
- The future direct detections XENONnT and LUX-ZEPLIN (LZ-7 2T) can give strong constraints to this scenario.
- The current indirect constraints to Higgs invisible decay $h_2 \rightarrow \tilde{\chi}_1^0 \tilde{\chi}_1^0$ are weak, but the direct detection of Higgs invisible decay at the future HL-LHC may cover half of the samples, and that of the CEPC may cover most.
- The branching ratio of Higgs exotic decay $h_2 \rightarrow h_1 h_1, a_1 a_1$ can be over 20 percent, while their contributions ($h_2 \rightarrow 4\tilde{\chi}_1^0$) to the invisible decay are very small.

Acknowledgments

This work was supported by the National Natural Science Foundation of China (NNSFC) under grant Nos. 11605123.

References

- [1] **ATLAS** Collaboration, G. Aad et al., *Observation of a new particle in the search for the Standard Model Higgs boson with the ATLAS detector at the LHC*, *Phys. Lett.* **B716** (2012) 1–29, [[arXiv:1207.7214](#)].
- [2] **CMS** Collaboration, S. Chatrchyan et al., *Observation of a New Boson at a Mass of 125 GeV with the CMS Experiment at the LHC*, *Phys. Lett.* **B716** (2012) 30–61, [[arXiv:1207.7235](#)].
- [3] **ATLAS** Collaboration, G. Aad et al., *Combined measurements of Higgs boson production and decay using up to 80 fb⁻¹ of proton-proton collision data at $\sqrt{s} = 13$ TeV collected with the ATLAS experiment*, *Phys. Rev.* **D101** (2020), no. 1 012002, [[arXiv:1909.02845](#)].
- [4] **CMS** Collaboration, C. Collaboration, *Combined Higgs boson production and decay measurements with up to 137 fb⁻¹ of proton-proton collision data at $\sqrt{s} = 13$ TeV*, .
- [5] **ATLAS, CMS** Collaboration, A. Sopczak, *Precision Measurements in the Higgs Sector at ATLAS and CMS*, in *International Conference on Precision Physics and Fundamental Physical Constants (FFK2019) Tihany, Hungary, June 9-14, 2019*, 2020. [arXiv:2001.05927](#).
- [6] **ATLAS** Collaboration, M. Aaboud et al., *Combination of searches for invisible Higgs boson decays with the ATLAS experiment*, *Phys. Rev. Lett.* **122** (2019), no. 23 231801, [[arXiv:1904.05105](#)].
- [7] **CMS** Collaboration, A. M. Sirunyan et al., *Search for invisible decays of a Higgs boson produced through vector boson fusion in proton-proton collisions at $\sqrt{s} = 13$ TeV*, *Phys. Lett.* **B793** (2019) 520–551, [[arXiv:1809.05937](#)].
- [8] J.-J. Cao, Z.-X. Heng, J. M. Yang, Y.-M. Zhang, and J.-Y. Zhu, *A SM-like Higgs near 125 GeV in low energy SUSY: a comparative study for MSSM and NMSSM*, *JHEP* **03** (2012) 086, [[arXiv:1202.5821](#)].
- [9] J.-J. Cao, Z. Heng, J. M. Yang, and J. Zhu, *Higgs decay to dark matter in low energy SUSY: is it detectable at the LHC ?*, *JHEP* **06** (2012) 145, [[arXiv:1203.0694](#)].
- [10] J. Cao, Z. Heng, J. M. Yang, and J. Zhu, *Status of low energy SUSY models confronted with the LHC 125 GeV Higgs data*, *JHEP* **10** (2012) 079, [[arXiv:1207.3698](#)].
- [11] K. Kowalska, S. Munir, L. Roszkowski, E. M. Sessolo, S. Trojanowski, and Y.-L. S. Tsai, *Constrained next-to-minimal supersymmetric standard model with a 126 GeV Higgs boson: A global analysis*, *Phys. Rev.* **D87** (2013) 115010, [[arXiv:1211.1693](#)].
- [12] J. F. Gunion, Y. Jiang, and S. Kraml, *The Constrained NMSSM and Higgs near 125 GeV*, *Phys. Lett.* **B710** (2012) 454–459, [[arXiv:1201.0982](#)].
- [13] U. Ellwanger, A. Florent, and D. Zerwas, *Discovering the constrained NMSSM with tau leptons at the LHC*, *JHEP* **01** (2011) 103, [[arXiv:1011.0931](#)].
- [14] G. Panotopoulos, *Gravitino dark matter with neutralino NLSP in the constrained NMSSM*, *J. Phys. Conf. Ser.* **259** (2010) 012064, [[arXiv:1010.4481](#)].
- [15] D. E. Lopez-Fogliani, L. Roszkowski, R. Ruiz de Austri, and T. A. Varley, *A Bayesian Analysis of the Constrained NMSSM*, *Phys. Rev.* **D80** (2009) 095013, [[arXiv:0906.4911](#)].
- [16] G. Belanger, C. Hugonie, and A. Pukhov, *Precision measurements, dark matter direct detection and LHC Higgs searches in a constrained NMSSM*, *JCAP* **0901** (2009) 023, [[arXiv:0811.3224](#)].

- [17] A. Djouadi, U. Ellwanger, and A. M. Teixeira, *Phenomenology of the constrained NMSSM*, *JHEP* **04** (2009) 031, [[arXiv:0811.2699](#)].
- [18] U. Ellwanger, *The Constrained NMSSM: $mSUGRA$ and $GMSB$* , *AIP Conf. Proc.* **1078** (2009), no. 1 73–78, [[arXiv:0809.0779](#)].
- [19] C. Hugonie, G. Belanger, and A. Pukhov, *Dark matter in the constrained NMSSM*, *JCAP* **0711** (2007) 009, [[arXiv:0707.0628](#)].
- [20] D. G. Cerdeño, V. De Romeri, V. Martín-Lozano, K. A. Olive, and O. Seto, *The Constrained NMSSM with right-handed neutrinos*, *Eur. Phys. J.* **C78** (2018), no. 4 290, [[arXiv:1707.03990](#)].
- [21] J. Cao, Z. Heng, D. Li, and J. M. Yang, *Current experimental constraints on the lightest Higgs boson mass in the constrained MSSM*, *Phys. Lett.* **B710** (2012) 665–670, [[arXiv:1112.4391](#)].
- [22] J. Ellis and K. A. Olive, *Revisiting the Higgs Mass and Dark Matter in the CMSSM*, *Eur. Phys. J.* **C72** (2012) 2005, [[arXiv:1202.3262](#)].
- [23] P. Bechtle et al., *Killing the $cMSSM$ softly*, *Eur. Phys. J.* **C76** (2016), no. 2 96, [[arXiv:1508.05951](#)].
- [24] **GAMBIT** Collaboration, P. Athron et al., *Global fits of GUT-scale SUSY models with GAMBIT*, *Eur. Phys. J.* **C77** (2017), no. 12 824, [[arXiv:1705.07935](#)].
- [25] K. Wang and J. Zhu, *The Light Higgsino-dominated NLSPs in the Semi-constrained NMSSM*, [arXiv:1911.08319](#).
- [26] K. Wang, F. Wang, J. Zhu, and Q. Jie, *The semi-constrained NMSSM in light of muon $g-2$, LHC, and dark matter constraints*, *Chin. Phys.* **C42** (2018), no. 10 103109–103109, [[arXiv:1811.04435](#)].
- [27] U. Ellwanger and C. Hugonie, *The semi-constrained NMSSM satisfying bounds from the LHC, LUX and Planck*, *JHEP* **08** (2014) 046, [[arXiv:1405.6647](#)].
- [28] D. Das, U. Ellwanger, and A. M. Teixeira, *LHC constraints on $M_{1/2}$ and m_0 in the semi-constrained NMSSM*, *JHEP* **04** (2013) 117, [[arXiv:1301.7584](#)].
- [29] U. Ellwanger and C. Hugonie, *The higgsino-singlino sector of the NMSSM: combined constraints from dark matter and the LHC*, *Eur. Phys. J.* **C78** (2018), no. 9 735, [[arXiv:1806.09478](#)].
- [30] U. Ellwanger, *Present Status and Future Tests of the Higgsino-Singlino Sector in the NMSSM*, *JHEP* **02** (2017) 051, [[arXiv:1612.06574](#)].
- [31] K. Nakamura and D. Nomura, *Charged Lepton Flavor Violation in the Semi-Constrained NMSSM with Right-Handed Neutrinos*, *Phys. Lett.* **B746** (2015) 396–405, [[arXiv:1501.05058](#)].
- [32] J. Ren, L. Wu, J. M. Yang, and J. Zhao, *Exploring supersymmetry with machine learning*, *Nucl. Phys.* **B943** (2019) 114613, [[arXiv:1708.06615](#)].
- [33] M. Abdughani, J. Ren, L. Wu, J. M. Yang, and J. Zhao, *Supervised deep learning in high energy phenomenology: a mini review*, *Commun. Theor. Phys.* **71** (2019), no. 8 955, [[arXiv:1905.06047](#)].
- [34] F. Staub, *$xBIT$: an easy to use scanning tool with machine learning abilities*, [arXiv:1906.03277](#).

- [35] I. J. Goodfellow, J. Pouget-Abadie, M. Mirza, B. Xu, D. Warde-Farley, S. Ozair, A. Courville, and Y. Bengio, *Generative Adversarial Networks*, [arXiv:1406.2661](#).
- [36] M. Paganini, L. de Oliveira, and B. Nachman, *CaloGAN : Simulating 3D high energy particle showers in multilayer electromagnetic calorimeters with generative adversarial networks*, *Phys. Rev.* **D97** (2018), no. 1 014021, [[arXiv:1712.10321](#)].
- [37] P. Musella and F. Pandolfi, *Fast and Accurate Simulation of Particle Detectors Using Generative Adversarial Networks*, *Comput. Softw. Big Sci.* **2** (2018), no. 1 8, [[arXiv:1805.00850](#)].
- [38] M. Erdmann, J. Glombitza, and T. Quast, *Precise simulation of electromagnetic calorimeter showers using a Wasserstein Generative Adversarial Network*, *Comput. Softw. Big Sci.* **3** (2019), no. 1 4, [[arXiv:1807.01954](#)].
- [39] R. Di Sipio, M. Fauci Giannelli, S. Ketabchi Haghighat, and S. Palazzo, *DijetGAN: A Generative-Adversarial Network Approach for the Simulation of QCD Dijet Events at the LHC*, *JHEP* **08** (2020) 110, [[arXiv:1903.02433](#)].
- [40] S. Otten, S. Caron, W. de Swart, M. van Beekveld, L. Hendriks, C. van Leeuwen, D. Podareanu, R. Ruiz de Austri, and R. Verheyen, *Event Generation and Statistical Sampling for Physics with Deep Generative Models and a Density Information Buffer*, [arXiv:1901.00875](#).
- [41] J. Lin, W. Bhimji, and B. Nachman, *Machine Learning Templates for QCD Factorization in the Search for Physics Beyond the Standard Model*, *JHEP* **05** (2019) 181, [[arXiv:1903.02556](#)].
- [42] A. Butter, T. Plehn, and R. Winterhalder, *How to GAN LHC Events*, *SciPost Phys.* **7** (2019) 075, [[arXiv:1907.03764](#)].
- [43] M. Bellagente, A. Butter, G. Kasieczka, T. Plehn, and R. Winterhalder, *How to GAN away Detector Effects*, [arXiv:1912.00477](#).
- [44] A. Butter, T. Plehn, and R. Winterhalder, *How to GAN Event Subtraction*, [arXiv:1912.08824](#).
- [45] D. J. Miller, R. Nevzorov, and P. M. Zerwas, *The Higgs sector of the next-to-minimal supersymmetric standard model*, *Nucl. Phys.* **B681** (2004) 3–30, [[hep-ph/0304049](#)].
- [46] M. Carena, H. E. Haber, I. Low, N. R. Shah, and C. E. M. Wagner, *Alignment limit of the NMSSM Higgs sector*, *Phys. Rev. D* **93** (2016), no. 3 035013, [[arXiv:1510.09137](#)].
- [47] U. Ellwanger, C. Hugonie, and A. M. Teixeira, *The Next-to-Minimal Supersymmetric Standard Model*, *Phys. Rept.* **496** (2010) 1–77, [[arXiv:0910.1785](#)].
- [48] D. Das, U. Ellwanger, and A. M. Teixeira, *Modified Signals for Supersymmetry in the NMSSM with a Singlino-like LSP*, *JHEP* **04** (2012) 067, [[arXiv:1202.5244](#)].
- [49] M. D. Zeiler, *Adadelata: an adaptive learning rate method*, *arXiv:1212.5701* (2012).
- [50] U. Ellwanger, J. F. Gunion, and C. Hugonie, *NMHDECAY: A Fortran code for the Higgs masses, couplings and decay widths in the NMSSM*, *JHEP* **02** (2005) 066, [[hep-ph/0406215](#)].
- [51] U. Ellwanger and C. Hugonie, *NMHDECAY 2.0: An Updated program for sparticle masses, Higgs masses, couplings and decay widths in the NMSSM*, *Comput. Phys. Commun.* **175** (2006) 290–303, [[hep-ph/0508022](#)].

- [52] U. Ellwanger and C. Hugonie, *NMSPEC: A Fortran code for the sparticle and Higgs masses in the NMSSM with GUT scale boundary conditions*, *Comput. Phys. Commun.* **177** (2007) 399–407, [[hep-ph/0612134](#)].
- [53] D. Das, U. Ellwanger, and A. M. Teixeira, *NMSDECAY: A Fortran Code for Supersymmetric Particle Decays in the Next-to-Minimal Supersymmetric Standard Model*, *Comput. Phys. Commun.* **183** (2012) 774–779, [[arXiv:1106.5633](#)].
- [54] **Particle Data Group** Collaboration, M. Tanabashi et al., *Review of Particle Physics*, *Phys. Rev.* **D98** (2018), no. 3 030001.
- [55] **LHCb** Collaboration, R. Aaij et al., *First Evidence for the Decay $B_s^0 \rightarrow \mu^+ \mu^-$* , *Phys. Rev. Lett.* **110** (2013), no. 2 021801, [[arXiv:1211.2674](#)].
- [56] **BaBar** Collaboration, J. P. Lees et al., *Evidence for an excess of $\bar{B} \rightarrow D^{(*)} \tau^- \bar{\nu}_\tau$ decays*, *Phys. Rev. Lett.* **109** (2012) 101802, [[arXiv:1205.5442](#)].
- [57] **BaBar** Collaboration, J. P. Lees et al., *Precision Measurement of the $B \rightarrow X_s \gamma$ Photon Energy Spectrum, Branching Fraction, and Direct CP Asymmetry $A_{CP}(B \rightarrow X_{s+d} \gamma)$* , *Phys. Rev. Lett.* **109** (2012) 191801, [[arXiv:1207.2690](#)].
- [58] **CMS** Collaboration, A. M. Sirunyan et al., *Combined measurements of Higgs boson couplings in proton–proton collisions at $\sqrt{s} = 13$ TeV*, *Eur. Phys. J.* **C79** (2019), no. 5 421, [[arXiv:1809.10733](#)].
- [59] **ATLAS, CMS** Collaboration, G. Aad et al., *Measurements of the Higgs boson production and decay rates and constraints on its couplings from a combined ATLAS and CMS analysis of the LHC pp collision data at $\sqrt{s} = 7$ and 8 TeV*, *JHEP* **08** (2016) 045, [[arXiv:1606.02266](#)].
- [60] **WMAP** Collaboration, G. Hinshaw et al., *Nine-Year Wilkinson Microwave Anisotropy Probe (WMAP) Observations: Cosmological Parameter Results*, *Astrophys. J. Suppl.* **208** (2013) 19, [[arXiv:1212.5226](#)].
- [61] **Planck** Collaboration, P. A. R. Ade et al., *Planck 2013 results. XVI. Cosmological parameters*, *Astron. Astrophys.* **571** (2014) A16, [[arXiv:1303.5076](#)].
- [62] G. Belanger, F. Boudjema, A. Pukhov, and A. Semenov, *MicrOMEGAs 2.0: A Program to calculate the relic density of dark matter in a generic model*, *Comput. Phys. Commun.* **176** (2007) 367–382, [[hep-ph/0607059](#)].
- [63] G. Belanger, F. Boudjema, A. Pukhov, and A. Semenov, *Dark matter direct detection rate in a generic model with micrOMEGAs 2.2*, *Comput. Phys. Commun.* **180** (2009) 747–767, [[arXiv:0803.2360](#)].
- [64] G. Belanger, F. Boudjema, A. Pukhov, and A. Semenov, *micrOMEGAs: A Tool for dark matter studies*, *Nuovo Cim.* **C033N2** (2010) 111–116, [[arXiv:1005.4133](#)].
- [65] G. Belanger, F. Boudjema, A. Pukhov, and A. Semenov, *micrOMEGAs_3: A program for calculating dark matter observables*, *Comput. Phys. Commun.* **185** (2014) 960–985, [[arXiv:1305.0237](#)].
- [66] **XENON** Collaboration, E. Aprile et al., *Dark Matter Search Results from a One Ton-Year Exposure of XENON1T*, *Phys. Rev. Lett.* **121** (2018), no. 11 111302, [[arXiv:1805.12562](#)].
- [67] **LUX** Collaboration, D. S. Akerib et al., *Results on the Spin-Dependent Scattering of Weakly Interacting Massive Particles on Nucleons from the Run 3 Data of the LUX Experiment*, *Phys. Rev. Lett.* **116** (2016), no. 16 161302, [[arXiv:1602.03489](#)].

- [68] **XENON** Collaboration, E. Aprile et al., *Constraining the spin-dependent WIMP-nucleon cross sections with XENON1T*, *Phys. Rev. Lett.* **122** (2019), no. 14 141301, [[arXiv:1902.03234](#)].
- [69] **PICO** Collaboration, C. Amole et al., *Dark Matter Search Results from the Complete Exposure of the PICO-60 C₃F₈ Bubble Chamber*, *Phys. Rev.* **D100** (2019), no. 2 022001, [[arXiv:1902.04031](#)].
- [70] **Muon g-2** Collaboration, G. W. Bennett et al., *Final Report of the Muon E821 Anomalous Magnetic Moment Measurement at BNL*, *Phys. Rev.* **D73** (2006) 072003, [[hep-ex/0602035](#)].
- [71] A. Czarnecki, W. J. Marciano, and A. Vainshtein, *Refinements in electroweak contributions to the muon anomalous magnetic moment*, *Phys. Rev.* **D67** (2003) 073006, [[hep-ph/0212229](#)]. [Erratum: *Phys. Rev.* **D73**, 119901(2006)].
- [72] S. Heinemeyer, D. Stockinger, and G. Weiglein, *Electroweak and supersymmetric two-loop corrections to $(g-2)(\mu)$* , *Nucl. Phys.* **B699** (2004) 103–123, [[hep-ph/0405255](#)].
- [73] J. Bijnens and J. Prades, *The Hadronic Light-by-Light Contribution to the Muon Anomalous Magnetic Moment: Where do we stand?*, *Mod. Phys. Lett.* **A22** (2007) 767–782, [[hep-ph/0702170](#)].
- [74] F. Jegerlehner, *Essentials of the Muon g-2*, *Acta Phys. Polon.* **B38** (2007) 3021, [[hep-ph/0703125](#)].
- [75] **CMS** Collaboration, A. M. Sirunyan et al., *Combined search for electroweak production of charginos and neutralinos in proton-proton collisions at $\sqrt{s} = 13$ TeV*, *JHEP* **03** (2018) 160, [[arXiv:1801.03957](#)].
- [76] S. Kraml, S. Kulkarni, U. Laa, A. Lessa, W. Magerl, D. Proschofsky, and W. Waltenberger, *SModelS: a tool for interpreting simplified-model results from the LHC and its application to supersymmetry*, *Eur. Phys. J.* **C74** (2014) 2868, [[arXiv:1312.4175](#)].
- [77] F. Ambrogio, S. Kraml, S. Kulkarni, U. Laa, A. Lessa, V. Magerl, J. Sonneveld, M. Traub, and W. Waltenberger, *SModelS v1.1 user manual*, [[arXiv:1701.06586](#)].
- [78] F. Ambrogio et al., *SModelS v1.2: long-lived particles, combination of signal regions, and other novelties*, [[arXiv:1811.10624](#)].
- [79] J. Dutta, S. Kraml, A. Lessa, and W. Waltenberger, *SModelS extension with the CMS supersymmetry search results from Run 2*, *LHEP* **1** (2018), no. 1 5–12, [[arXiv:1803.02204](#)].
- [80] A. Buckley, *PySLHA: a Pythonic interface to SUSY Les Houches Accord data*, [[arXiv:1305.4194](#)].
- [81] T. Sjöstrand, S. Mrenna, and P. Z. Skands, *PYTHIA 6.4 Physics and Manual*, *JHEP* **0605** (2006) 026, [[hep-ph/0603175](#)].
- [82] T. Sjöstrand, S. Ask, J. R. Christiansen, R. Corke, N. Desai, P. Ilten, S. Mrenna, S. Prestel, C. O. Rasmussen, and P. Z. Skands, *An Introduction to PYTHIA 8.2*, *Comput. Phys. Commun.* **191** (2015) 159–177, [[arXiv:1410.3012](#)].
- [83] P. Bechtle, S. Heinemeyer, O. Stal, T. Stefaniak, and G. Weiglein, *Applying Exclusion Likelihoods from LHC Searches to Extended Higgs Sectors*, *Eur. Phys. J.* **C75** (2015), no. 9 421, [[arXiv:1507.06706](#)].
- [84] P. Bechtle, O. Brein, S. Heinemeyer, O. Stål, T. Stefaniak, G. Weiglein, and K. E. Williams,

HiggsBounds – 4: Improved Tests of Extended Higgs Sectors against Exclusion Bounds from LEP, the Tevatron and the LHC, *Eur. Phys. J.* **C74** (2014), no. 3 2693, [[arXiv:1311.0055](#)].

- [85] P. Bechtle, O. Brein, S. Heinemeyer, O. Stal, T. Stefaniak, G. Weiglein, and K. Williams, *Recent Developments in HiggsBounds and a Preview of HiggsSignals*, *PoS CHARGED2012* (2012) 024, [[arXiv:1301.2345](#)].
- [86] P. Bechtle, O. Brein, S. Heinemeyer, G. Weiglein, and K. E. Williams, *HiggsBounds 2.0.0: Confronting Neutral and Charged Higgs Sector Predictions with Exclusion Bounds from LEP and the Tevatron*, *Comput. Phys. Commun.* **182** (2011) 2605–2631, [[arXiv:1102.1898](#)].
- [87] P. Bechtle, O. Brein, S. Heinemeyer, G. Weiglein, and K. E. Williams, *HiggsBounds: Confronting Arbitrary Higgs Sectors with Exclusion Bounds from LEP and the Tevatron*, *Comput. Phys. Commun.* **181** (2010) 138–167, [[arXiv:0811.4169](#)].
- [88] J. Billard, L. Strigari, and E. Figueroa-Feliciano, *Implication of neutrino backgrounds on the reach of next generation dark matter direct detection experiments*, *Phys. Rev.* **D89** (2014), no. 2 023524, [[arXiv:1307.5458](#)].
- [89] Z. Liu, L.-T. Wang, and H. Zhang, *Exotic decays of the 125 GeV Higgs boson at future e^+e^- lepton colliders*, *Chin. Phys.* **C41** (2017), no. 6 063102, [[arXiv:1612.09284](#)].
- [90] Y. Tan, X. Shi, R. Kiuchi, M. Ruan, M. Jing, X. Mo, X. Lou, G. Li, K. Zhang, and S. Jyotishmati, *Search for invisible decay of a Higgs boson produced at the CEPC*, [arXiv:2001.05912](#).
- [91] D. d’Enterria, *Higgs physics at the Future Circular Collider*, *PoS ICHEP2016* (2017) 434, [[arXiv:1701.02663](#)].
- [92] A. Ishikawa, *Search for invisible decays of the Higgs boson at the ILC*, *PoS LeptonPhoton2019* (2019) 147, [[arXiv:1909.07537](#)].
- [93] K. Wang and J. Zhu, *Funnel annihilations of light dark matter and the invisible decay of the Higgs boson*, [arXiv:2003.01662](#).
- [94] ATLAS Collaboration, M. Aaboud et al., *Search for additional heavy neutral Higgs and gauge bosons in the ditau final state produced in 36 fb^{-1} of pp collisions at $\sqrt{s} = 13\text{ TeV}$ with the ATLAS detector*, *JHEP* **01** (2018) 055, [[arXiv:1709.07242](#)].
- [95] CMS Collaboration, A. M. Sirunyan et al., *Search for additional neutral MSSM Higgs bosons in the $\tau\tau$ final state in proton-proton collisions at $\sqrt{s} = 13\text{ TeV}$* , *JHEP* **09** (2018) 007, [[arXiv:1803.06553](#)].